# Phonon-assisted cooperative sensitization of $Tb^{3+}$ in $SrCl_2$:Yb, Tb



2002 J. Phys.: Condens. Matter 14 5461

(http://iopscience.iop.org/0953-8984/14/22/301)

INSTITUTE OF PHYSICS PUBLISHING JOURNAL OF PHYSICS: CONDENSED MATTER

J. Phys.: Condens. Matter **14** (2002) 5461–5475 PII: S0953-8984(02)35100-2

# Phonon-assisted cooperative sensitization of $Tb^{3+}$ in $SrCl_2$:Yb, Tb

**G M Salley[1], R Valiente[2] and H U Güdel[1]**

[1] Departement für Chemie and Biochemie, Universität Bern, Freiestrasse 3, CH-3000 Bern 9, Switzerland
[2] Departamento de Física Aplicada, Facultad de Ciencias, Universidad de Cantabria, 39005 Santander, Spain

E-mail: hans-ulrich.guedel@iac.unibe.ch

Received 20 March 2002, in final form 25 April 2002
Published 23 May 2002
Online at stacks.iop.org/JPhysCM/14/5461

**Abstract**

Excitation into the $Yb^{3+}$ $^2F_{5/2}$ excited states leads to visible-by-eye green luminescence spanning the spectral region from 490 to 790 nm, with a quadratic power dependence. Optical absorption, luminescence, and excitation spectroscopy as well as pulsed measurements on single-crystal $SrCl_2$:Yb(1%), Tb(1%) are used to determine the upconversion (UC) properties of this system. The upconverted luminescence is easily detectable by eye from RT to 100 K, at which point the intensity drops significantly and a change in colour from green to blue is observed. Pulsed measurements coupled with excitation spectroscopy lead to the unambiguous assignment of a phonon-assisted cooperative sensitization mechanism as the dominant UC process for $T > 50$ K with $\frac{\text{VIS}}{\text{NIR}}$ photon ratios on the order of $10^{-2}$% for a laser power of 56 W mm$^{-2}$. Below 50 K, the dominant UC emission becomes the well-known Yb–Yb cooperative luminescence around 500 nm, with a consequential reduction of $Tb^{3+}$ emission by more than three orders of magnitude from RT to 10 K.

## 1. Introduction

The upconversion (UC) of low-energy photons to high-energy photons is a well-studied phenomenon which now has use in many applications. These include solid-state lasers, phosphor materials, optical data storage, IR counters, among other devices which have the advantage of cheap and readily available excitation sources, namely IR diodes, as well as consisting of all solid-state components [1]. The key to synthesizing new and improved UC devices relies on the fundamental understanding of the principles which govern the UC process. The $Yb^{3+}$-sensitized UC luminescence of $Tb^{3+}$ ions has been studied for many years and has

  

even been proposed by previous authors as a system which could potentially produce laser action [2, 3]. Using $Yb^{3+}$ as a sensitizer ion is attractive because of the relatively strong oscillator strength of the $Yb^{3+}$ $^2F_{7/2} \rightarrow {}^2F_{5/2}$ transitions, which are in the near-infrared (NIR) range of inexpensive efficient solid-state diode lasers. In addition, the $^2F_{5/2}$ state has a quantum efficiency near to 1 in ionic lattices. Additionally, the $Tb^{3+}$ ion is attractive as the active emitting ion because of its broad emission range, allowing tunability in the visible, and its tendency to relax radiatively instead of through non-radiative channels, such as cross-relaxation or multi-phonon decay, which would reduce the quantum efficiency away from the theoretical limit of 50% for UC processes. Although the Yb:Tb UC system was introduced in 1969, there is still some debate as to what is the dominant process which converts low-energy photons into higher-energy visible photons [2, 4, 5]. Therefore the focus of this paper is on gaining a better understanding of the Yb:Tb system and determining the dominant UC mechanism.

The confusion about UC in the Yb:Tb system arises because it can not be explained with the 'normal' UC mechanisms for heterogeneous systems, i.e. systems which involve two different ions. The reason is that $Yb^{3+}$ has only one excited state, $^2F_{5/2}$ around 10 000 $cm^{-1}$, and $Tb^{3+}$ does not have any excited states in this spectral range. The two mechanisms proposed by previous authors to describe the UC are cooperative sensitization and the so-called GSA/ESA (ground-state absorption/excited-state absorption). The former involves energy transfer from two excited $Yb^{3+}$ ions, called the sensitizer, simultaneously to the $Tb^{3+}$ ion, called the activator. The GSA/ESA process involves a $^2F_{7/2} \rightarrow {}^2F_{5/2}$ ground-state absorption of the $Yb^{3+}$ ion followed by an excited-state absorption from the $Yb^{3+}$ meta-stable level to the $Tb^{3+}$ meta-stable level. These two processes, which will be discussed in greater detail later, have the same characteristics as the well-known GSA/ETU (ground-state absorption/energy transfer UC) and GSA/ESA, respectively, which describe homogeneous systems involving only one chromophore. To distinguish between GSA/ETU and GSA/ESA, two standard techniques are generally used, namely short-pulse measurements and excitation spectroscopy [6]. We apply these two techniques to the Yb:Tb system to determine the dominant UC mechanism.

We have chosen $SrCl_2$:Yb(1%), Tb(1%) for this study because of the tendency of rare-earth (RE) ions to group together due to the charge mismatch of substituting a trivalent ion for a divalent host ion [7]. This grouping of ions can be advantageous for UC involving energy transfer, since this process requires interactions between the active ions and is therefore dependent upon their distance [8].

It is important to note that energy conservation dictates for cooperative sensitization that the energy of the relevant activator ion level, $Tb^{3+}$ $^5D_4$, must be less than or equal to twice the sensitizer energy level, $Yb^{3+}$ $^2F_{5/2}$. This requirement is often not satisfied in Yb:Tb compounds, including the title compound. The small energy gap between these levels, however, can be bridged by phonons, and therefore the UC luminescence in this system is strongly dependent on the temperature of the crystal, as will be discussed in section 4.3.2.

We present results of pulsed and CW spectroscopy performed on $SrCl_2$:Yb, Tb which lead to the clear assignment of a phonon-assisted cooperative sensitization mechanism responsible for $Tb^{3+}$ luminescence under $Yb^{3+}$ excitation above 50 K. The UC luminescence temperature dependence is presented to determine the activation energy of the process. An activation energy of 150 $cm^{-1}$ is found which is equal to the energy difference between the lowest $Tb^{3+}$ $^5D_4$ crystal-field level and two times the lowest crystal-field level of $Yb^{3+}$ $^2F_{5/2}$. The rate constant associated with the energy transfer is determined by pulsed measurement with $1 \times 10^7$ W $mm^{-2}$ at 10 190 $cm^{-1}$ and analysis through rate equations to be 2000 $s^{-1}$ at 100 K. It is discussed in terms of dynamical considerations as well as the efficiency of the UC process. We also show and briefly discuss the two dominant crystal-field sites for $Yb^{3+}$ in this lattice which both contribute to the $Tb^{3+}$ UC luminescence at high temperatures.

## 2. Experimental techniques

### *2.1. Synthesis of $SrCl_2$:Yb, Tb*

Stoichiometric amounts of $SrCl_2$, $TbCl_3$, and $YbCl_3$ precursors were mixed, fired to 890 °C, and single crystals were grown via the Bridgman technique. The $TbCl_3$ and $YbCl_3$ starting materials were prepared from $Tb_4O_7$ (99.9999%), $Yb_2O_3$ (99.9999%), $NH_4Cl$ (>99.9%), and HCl (47%) by the ammonium halide method [9, 10]. The $SrCl_2$ was prepared from $SrCO_3$ (99.994%) by dissolving in HCl and adding $NH_4Cl$. The product was dried and decomposed under heating in vacuum in analogy with the ammonium halide method. At all stages of growth and handling, the samples were kept in an inert atmosphere of either vacuum, He, or $N_2$, to prevent the adsorption of water. Absorption measurements were performed on a 0.4 cm long clear crystal, which was cut, polished, and sealed in a copper cell with optical windows filled with He gas. Since $SrCl_2$ is cubic, a random orientation and unpolarized light could be used. Samples for luminescence measurements were sealed in quartz ampoules with a low-pressure atmosphere of He gas. The concentration of dopant ions is nominally 1% for both, and from the strength of absorption transitions the actual concentration is estimated to be close to this for both $Yb^{3+}$ and $Tb^{3+}$ [11].

### *2.2. Spectroscopy*

The absorption spectra were recorded on a Cary 5e spectrophotometer coupled with a closed-cycle cryogenic refrigerator (Varian) for cooling. Cooling for luminescence measurements was achieved via quartz He gas flow-tubes. Luminescence of the sample was excited via an $Ar^+$-ion laser (Spectra Physics 2060-10 SA) or with a Ti:sapphire laser (Spectra Physics 3900S), pumped by the same $Ar^+$-ion laser, for $Tb^{3+}$ luminescence and Yb/UC luminescence, respectively. The emission was dispersed through a 0.85 m double monochromator (Spex 1402) with 500 nm blazed 1200 groves $mm^{-1}$ gratings and detected with a cooled red-sensitive photomultiplier tube (Hamamatsu 3310-01). A Stanford Research SR-400 photon counter was used with a PC for data collection. The excitation laser beam was focused using an $f = 53$ mm lens. All spectra are presented as photons $s^{-1}$ versus $cm^{-1}$ and are corrected for the throughput of the detection system, the detector response, and for the index of refraction of air.

Kinetic measurements were performed with either the same excitation sources as described above coupled through an acousto-optical modulator (Coherent 305, Stanford Research DS 345 function generator) or the Raman-shifted (Quanta Ray, RS-1, $H_2$, 340 p.s.i.) output of a dye laser (Lambda Physik FL 3002, pyridine 1 in methanol) pumped with the second harmonic of a Nd:YAG laser (Quanta Ray DCR 3). The luminescence was dispersed through a 0.75 m single monochromator (Spex 1702) with a 750 nm blazed 600 grooves $mm^{-1}$ grating and detected with the same PMTs as above, coupled with a multichannel scaler (Stanford Research SR 430).

## 3. Results

The survey absorption, (a), and emission spectra, (b), are presented in figure 1. Sharp lines in the low-energy range of the absorption spectrum below 6000 $cm^{-1}$ are transitions within the $Tb^{3+}$ $^7F_J$ manifold, and the lines located around 10 000 $cm^{-1}$ are due to $^2F_{7/2} \rightarrow {}^2F_{5/2}$ transitions of $Yb^{3+}$. The $Tb^{3+}$ $^7F_6 \rightarrow {}^5D_4$ transition is expanded by a factor of 100 and is located around 20 500 $cm^{-1}$. At higher energy, f–d transitions of an $Yb^{2+}$ impurity are observed [12]. Both emission spectra (upside down) are excited with 10 626 $cm^{-1}$ (56 W $mm^{-2}$) light at $T = 100$ K. The emission around 10 000 $cm^{-1}$ is due to the $Yb^{3+}$ $^2F_{5/2} \rightarrow {}^2F_{7/2}$ transition

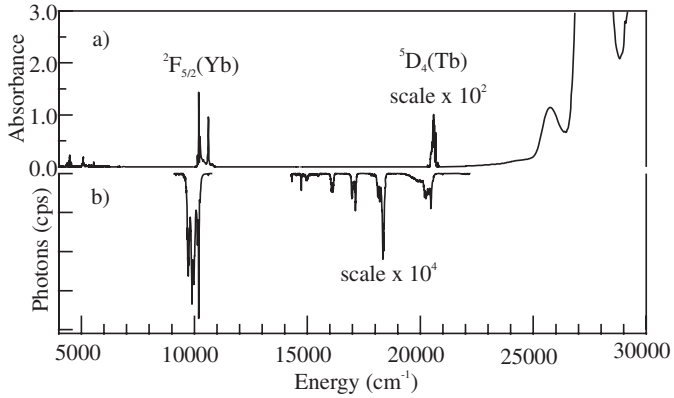


**Figure 1.** (a) The survey absorption spectrum of $SrCl_2$:Yb, Tb at 10 K. The $Tb^{3+}$ $^7F_6 \rightarrow {}^5D_4$ absorption has been scaled up by $10^2$. (b) The luminescence spectrum at 100 K under an excitation energy of 10 626 cm$^{-1}$ plotted upside down. The $Tb^{3+}$ $^5D_4 \rightarrow {}^7F_6$ luminescence has been scaled up by $10^4$.

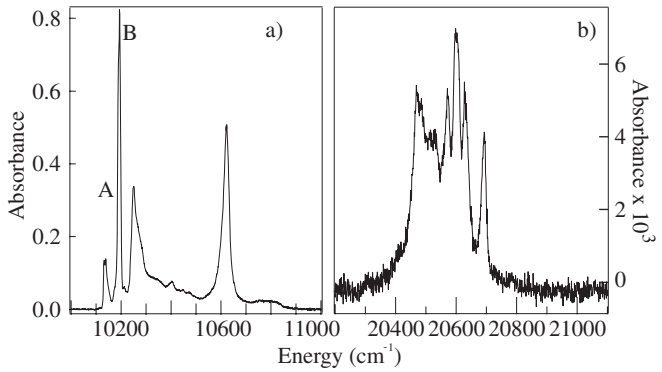


**Figure 2.** Absorption spectra for $Yb^{3+}$ $^2F_{7/2} \rightarrow {}^2F_{5/2}$, (a), and $Tb^{3+}$ $^7F_6 \rightarrow {}^5D_4$, (b), transitions at 15 K. Transitions for different $Yb^{3+}$ sites are labelled. Note the broken energy axis between (a) and (b).

and is $1 \times 10^4$ times stronger than the total of the five $Tb^{3+}$ $^5D_4 \rightarrow {}^7F_J$ emissions between 14 000 and 20 500 cm$^{-1}$ under the same excitation conditions.

High-resolution absorption spectra are presented in figure 2 for $Yb^{3+}$ $^2F_{7/2} \rightarrow {}^2F_{5/2}$ transitions, (a), and for $Tb^{3+}$ $^7F_6 \rightarrow {}^5D_4$ transitions (b). The spectra were taken with a 0.4 cm thick sample at 15 K. Absorption lines corresponding to two different $Yb^{3+}$ sites are labelled A and B.

$Yb^{3+}$ IR emission spectra with excitation at 10 138 cm$^{-1}$ (site A in figure 2) and 10 192 cm$^{-1}$ (site B in figure 2), at $T = 10$ K, are shown in figures 3(a) and (b) respectively. The spectrum in (a) represents emission from only site A, while the spectrum in (b) shows emission from both sites.

The $Yb^{3+}$ and $Tb^{3+}$ luminescence decays at $T = 100$ K are plotted in a semi-log plot in figure 4. Square-wave pulses at 10 626 cm$^{-1}$ were used for $Yb^{3+}$ while detecting luminescence at 10 192 cm$^{-1}$ (site B). 10 138 cm$^{-1}$ light was used for excitation into $Yb^{3+}$ site A (not shown) while detecting luminescence around 10 000 cm$^{-1}$. $Tb^{3+}$ luminescence was excited directly (20 486 cm$^{-1}$, solid) and by UC (10 626 cm$^{-1}$, dashed). The excitation power was

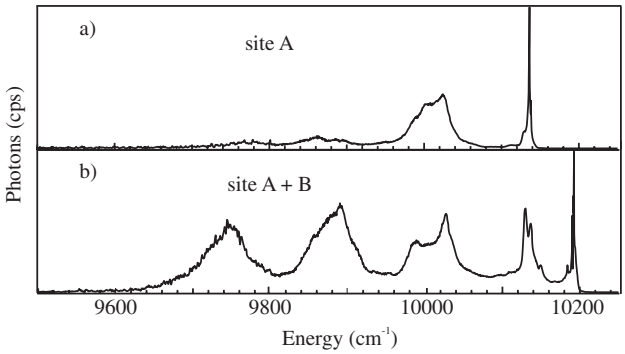


**Figure 3.** High-resolution luminescence spectra of $Yb^{3+}$ at 10 K with excitation energies of 10 138 and 10 192 $cm^{-1}$ for (a) and (b), respectively.

**Table 1.** Lifetimes of different levels. The values are calculated using the decay rate constants determined from figure 4.

| | $\tau$ (ms) $\pm 1\%$ | | |
|---|---|---|---|
| Level | 10 K | 100 K | 300 K |
| $^2F_{5/2}$, site A | 0.46 | 0.48 | 0.47 |
| $^2F_{5/2}$, site B | 0.53 | 0.50 | 0.47 |
| $^5D_4$ | 2.5 | 2.5 | 2.5 |
| $^5D_4$[a] | 2.2 | 2.1 | 1.9 |

[a] Lifetime determined under UC excitation conditions.

0.56 W $mm^{-2}$ for direct and 56 W $mm^{-2}$ for UC. All the decays are single exponential, and the lifetimes derived from these experiments are presented in table 1.

Figure 5 displays the temperature-dependent $Tb^{3+}$ luminescence spectra under two different excitation energies, $\tilde{\nu}_{exc} = 10\,626$ $cm^{-1}$ and $\tilde{\nu}_{exc} = 20\,486$ $cm^{-1}$, for (a) and (b) respectively. All spectra are independently normalized. The temperature dependence of the intensities will be presented in figure 8.

The UC excitation spectrum (a) and the square of the $Yb^{3+}$ absorption spectrum (b) for $T = 100$ K are plotted in figure 6. The excitation spectrum is obtained by scanning the Ti:sapphire laser through the $Yb^{3+}$ absorption region while monitoring the UC luminescence intensity at 18 360 $cm^{-1}$. The GSA spectrum presented in (b) has been squared due to the quadratic dependence of the UC luminescence on the excitation power. (c) and (d) display the power dependence of the $Yb^{3+}$ and $Tb^{3+}$ UC luminescence for excitation at 10 626 $cm^{-1}$ (site B) and detecting at 10 000 and 18 360 $cm^{-1}$ respectively. The $Yb^{3+}$ luminescence power dependence, (c), is found to have a slope of 1.0, while the line through the points in (d) is a linear regression with a slope close to 2, representing the two-photon nature of the UC process.

Figure 7 displays the UC luminescence ($\tilde{\nu}_{det} = 18\,360$ $cm^{-1}$) temporal response for 8 ns pulsed excitations into the $Yb^{3+}$ $^2F_{7/2} \rightarrow {}^2F_{5/2}$ absorption at 10 192 $cm^{-1}$ (site B) at $T = 100$ K, for a peak power estimated to be $1 \times 10^7$ W $mm^{-2}$. There is a clear rise of the UC luminescence which can be better seen in the inset (b). Part (c) is a semi-logarithmic plot which highlights the single-exponential nature of the decay part of the transient.

Temperature-dependent UC luminescence spectra are plotted in figure 8(a) where each curve is corrected for the square of the absorption cross-section at the excitation wavelength,

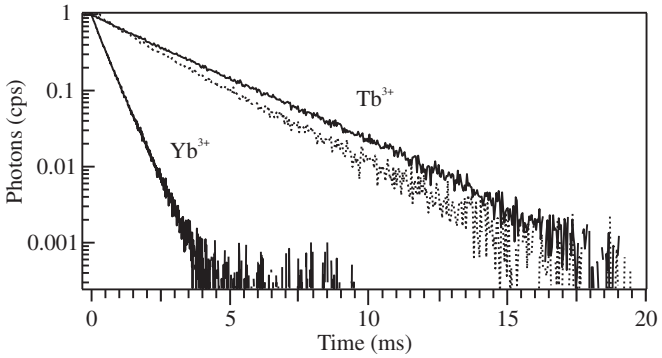


**Figure 4.** Responses of $Tb^{3+}$ and $Yb^{3+}$ luminescence intensities at 100 K under square-wave excitation energies of 20 486 and 10 626 $cm^{-1}$, respectively, in a semi-logarithmic representation. The dashed data represent the $Tb^{3+}$ luminescence decay after square-wave UC excitation at 10 626 $cm^{-1}$. The lifetimes of $Tb^{3+}$ and the two $Yb^{3+}$ sites can be found in table 1.

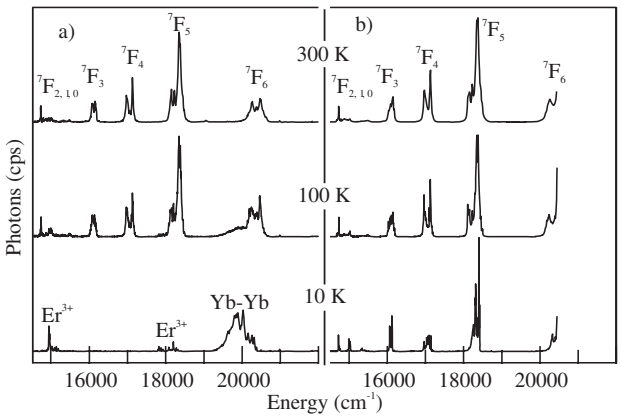


**Figure 5.** Luminescence spectra of $SrCl_2$:Yb, Tb at three temperatures produced by: (a) UC excitation at 10 626 $cm^{-1}$ and (b) direct excitation at 20 486 $cm^{-1}$. The spectra are not on the same *y*-axis scale.

$\tilde{\nu}_{exc} = 10\,626\ cm^{-1}$ (site B) (56 W $mm^{-2}$). The laser power and energy are kept constant for all the spectra. The correction is made because the UC process is a two-photon process—see figure 6(d)—and thus it is dependent upon the square of the absorbed photons. From 10 K to RT the UC intensity increases by more than three orders of magnitude, as shown in figure 8(b).

## 4. Discussion and analysis

### *4.1. $SrCl_2$ and trivalent dopant ions*

$SrCl_2$ crystallizes in the space group $O_h$ with the fluorite structure. The $Sr^{2+}$ ions are surrounded by eight $Cl^-$ ions with cubic coordination [13]. The introduction of trivalent RE ions into this structure, substituting for divalent Sr ions, has been studied and it has been determined that, in addition to the many possible single-ion sites due to different local and distant charge compensation possibilities, these dopant ions tend to form clusters [7]. And these clusters form at lower concentrations than in other fluorite crystals. Wietfeldt and Wright [13] determine that

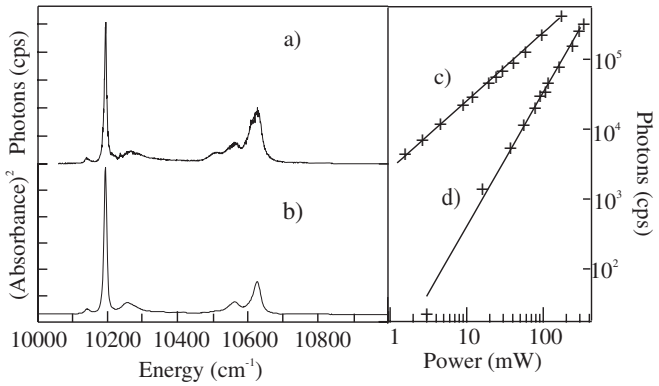


**Figure 6.** The 100 K UC luminescence excitation spectrum, monitoring 18 360 $cm^{-1}$ luminescence, is plotted in (a). The square of the ground-state absorption spectrum of $Yb^{3+}$ at 100 K is plotted in (b) for comparison. (c) and (d) are log–log intensity versus power representations at 100 K of the $Yb^{3+}$ emission at 10 000 $cm^{-1}$ and the $Tb^{3+}$ UC emission at 18 360 $cm^{-1}$, respectively. The excitation energy is 10 626 $cm^{-1}$ for both. The lines through the data points are linear regression fits with slopes of 1.0 (±0.05) and 1.9 (±0.1) respectively.

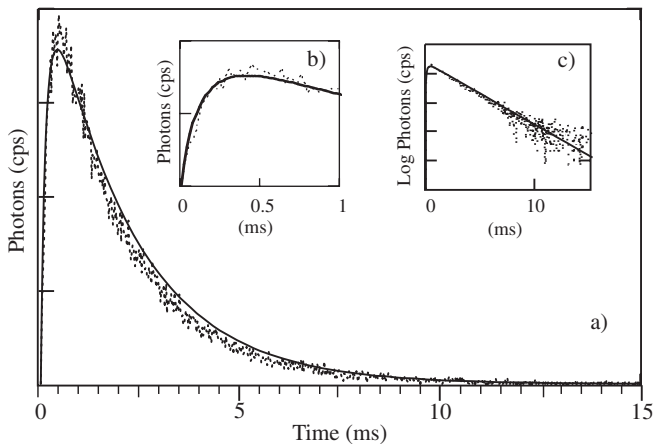


**Figure 7.** UC luminescence transient response, monitored at 18 360 $cm^{-1}$, after 8 ns pulsed excitation at 10 192 $cm^{-1}$ for $T = 100$ K (dashed data). The inset (b) shows the same data on an expanded $x$-axis. Inset (c) shows the same data in a log–linear representation. The solid curves in all plots are simulations using equations (1*a*)–(1*d*) with parameter values found in table 2.

for a $Eu^{3+}$ dopant concentration of $3 \times 10^{-3}$ mol% the cluster sites are already the dominant sites with two of the six identified sites being dominant at higher concentrations. It was also shown that the energy transfer between ions was greatly enhanced due to this clustering of ions. These conditions are ideal for UC processes involving interactions between different ions such as for $Tb^{3+}$ and $Yb^{3+}$.

This clustering of ions manifests itself in the optical spectra as inhomogeneously broadened absorption and emission bands [14]. There are four broad (∼10–40 $cm^{-1}$) $Yb^{3+}$ absorption features, for $T = 15$ K, observed at 10 138, 10 192, 10 270, and 10 626 $cm^{-1}$ (figure 2(a)). The two low-energy lines are assigned to the $^2F_{7/2}(0) \rightarrow {}^2F_{5/2}(0')$ transitions for two different sites labelled A and B respectively. Due to the width of the higher-lying bands and the fact that they

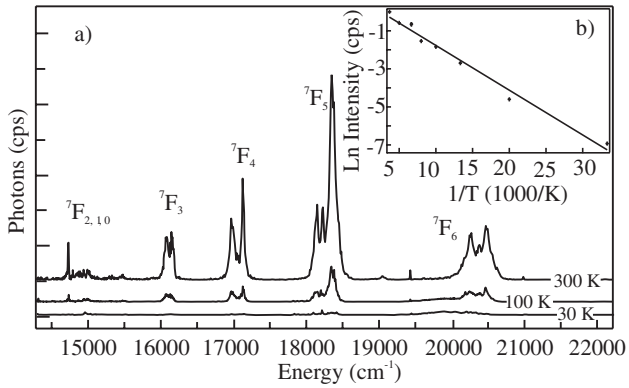


**Figure 8.** (a) The UC luminescence spectra for temperatures of 30, 100, and 300 K. Each spectrum has been divided by the corresponding square of the absorption cross-section at the excitation energy of 10 626 cm$^{-1}$. (b) An Arrhenius plot of the natural logarithm of the normalized total UC luminescence intensity versus the inverse of the temperature times 1000. The solid line is a fit using equation (3) described in the text.

overlap in energy, it is not possible to define clearly the crystal-field splitting of the $^2F_{5/2}$ level for each site. From the absorption spectrum we estimate that 14% of the ions are located on site A while 86% are located on site B. This estimate assumes equal oscillator strengths for the $^2F_{7/2} \rightarrow {}^2F_{5/2}$ transition at each site, which is reasonable considering the similar lifetimes of the levels; see table 1. Wietfeldt and Wright [13] found that in $SrCl_2$:Eu two defect sites were dominant at high concentrations in agreement with our results. The emission spectrum of site A is shown in figure 3(a). Excitation into site B, (b), leads to emission from both site A and site B due to partial energy transfer from B to A. Again it is difficult to determine the crystal-field splitting of the $^2F_{7/2}$ ground states with any accuracy, but there are clear differences between the two spectra. The broad band located at 10 010 cm$^{-1}$ is associated with site A while the two bands located around 9750 and 9880 cm$^{-1}$ are clearly associated with transitions involving $Yb^{3+}$ on site B. The energetic positions of these luminescence peaks correspond roughly to crystal-field levels of $Yb^{3+}$ in $Cs_2NaYbCl_6$ [15–17].

The $Tb^{3+}$ absorption spectrum, figure 2(b), is also broad and difficult to assign accurately. Relatively sharp transitions are observed in the region spanning 20 460 to 20 700 cm$^{-1}$ which are assigned to $^7F_6 \rightarrow {}^5D_4$ ground-state absorption transitions. For our study we are interested in the lowest-energy transition located at 20 468 cm$^{-1}$, which will be important in section 4.3.2 when discussing the temperature dependence of the UC luminescence. The energetic position of the four lowest peaks in the $Tb^{3+}$ absorption spectrum of figure 2(b) is similar to energies found in $Cs_2NaTbCl_6$ [15–17].

Decay time measurements for both $Tb^{3+}$ $^5D_4$ and $Yb^{3+}$ $^2F_{5/2}$ levels are presented in figure 4, for 100 K. The $Tb^{3+}$ $^5D_4$ lifetime stays constant between 10 and 300 K—see table 1—and we conclude that it is radiative. The same is true for the $Yb^{3+}$ site A luminescence lifetime. The $Yb^{3+}$ site B lifetime, on the other hand, changes with temperature and depends on the excitation and detection energy. At 10 K, $\tau_A = 0.46$ ($\pm 0.01$) ms, while the lifetime of site B is longer, with $\tau_B = 0.53$ ($\pm 0.01$) ms. As the temperature is raised, $\tau_B$ decreases and reaches a value which is comparable to that for site A. This reduction in lifetime with temperature is due to increasing energy transfer from B to A as the transfer process becomes more probable at higher temperatures. This energy transfer is also evident in figure 3 where excitation into site B leads to emission which contains features of both sites. From this spectrum we estimate that 40%

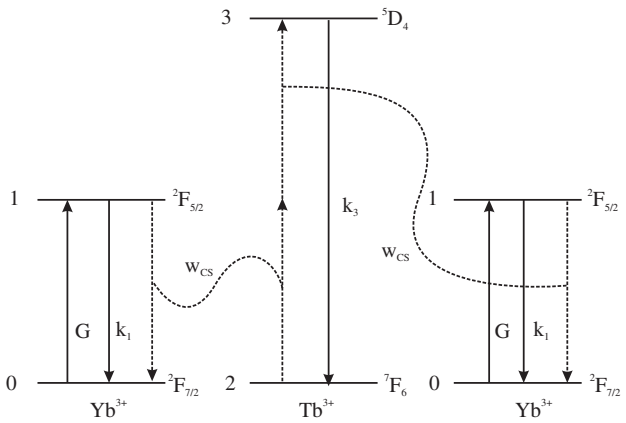


**Figure 9.** A diagram representing the cooperative sensitization of $Tb^{3+}$ luminescence by two excited $Yb^{3+}$ ions. The solid arrows represent radiative transitions and the dashed arrows represent non-radiative transitions involving energy transfer. The parameters in the diagram are described in the text and correspond to the parameters used in equation (1).

of the excitation into site B is transferred to site A at 10 K. Efficient energy transfer between $Yb^{3+}$ ions was also found in previous studies [13, 18].

### *4.2. Upconversion mechanism*

*4.2.1. General considerations.* The typical UC process, of heterogeneous systems, involves first an excitation of one ion, called the sensitizer. The energy is then transferred from the sensitizer to the second ion, called the activator, via a resonant or non-resonant energy transfer process. The activator is then further excited to a higher meta-stable state through a second energy transfer from a sensitizer. This process can be very efficient and some UC laser systems have been built on this principle using $Yb^{3+}$ as the sensitizer ion [1]. It is clear from the $Yb^{3+}$ and $Tb^{3+}$ energy levels that this process cannot be responsible for the UC observed after excitation to the $Yb^{3+}$ ion [19]. The excited meta-stable state of $Yb^{3+}$ lies around 10 000 $cm^{-1}$ whereas the $Tb^{3+}$ levels closest in energy to this are at 6000 and 20 000 $cm^{-1}$. Energy transfer to the 6000 $cm^{-1}$ level of $Tb^{3+}$, in addition to being highly off-resonant and therefore unlikely, cannot lead to UC as the second quantum of $Yb^{3+}$ $^2F_{7/2} \rightarrow {}^2F_{7/2}$ excitation will then not be sufficient in energy to excite the $Tb^{3+}$ to the higher meta-stable level, 20 000 $cm^{-1}$.

Due to the failure to explain the UC in Yb:Tb via standard processes, Ovsyankin and Feofilov [20] proposed the cooperative sensitization process. The cooperative sensitization mechanism involves the absorption of two NIR photons by two $Yb^{3+}$ ions and subsequently the simultaneous energy transfer from the $Yb^{3+}$ ions to a close $Tb^{3+}$ ion:

$$2 \times Yb^{3+}(^2F_{5/2}){:}Tb^{3+}(^7F_6) \Rightarrow 2 \times Yb^{3+}(^2F_{7/2}){:}Tb^{3+}(^5D_4).$$

A model of this process for the Yb:Tb system is presented in figure 9. This process was considered to be the dominant mechanism in the first study of Yb:Tb UC by Livanova *et al* [4]. The study was performed on doped $CaF_2$, and $SrF_2$ crystals, and assignment of the UC mechanism was based on the efficiency of the process. Later papers made similar assignments with different evidence such as the rise in UC intensity after a short excitation pulse into the $Yb^{3+}$ excited states [2, 21–26]. The rise after a short pulse is a well-known fingerprint

of an energy transfer process which needs no light to proceed and therefore continues after the laser pulse. Besides the short-pulse experiment, excitation spectroscopy can be used to assign a GSA/ETU mechanism. An excitation spectrum of UC luminescence governed by a GSA/ETU-type mechanism should resemble the square of the ground-state absorption to the intermediate level. This can be understood by considering the model in figure 9 and noting that the solid upward-pointing arrows, which represent absorption transitions which lead to UC luminescence, only concern transitions to the intermediate level. Since it takes two of these transitions for the UC to proceed, the excitation spectrum follows the square of the ground-state absorption of the sensitizer ion.

Other reports in the literature have assigned the UC mechanism to a GSA/ESA-type mechanism [2, 27]. This process proceeds through a sequence of two cooperative absorption steps:

$$\mathrm{Yb^{3+}}(^2\mathrm{F}_{7/2}):\mathrm{Tb^{3+}}(^7\mathrm{F}_6) + \text{photon} \Rightarrow \mathrm{Yb^{3+}}(^2\mathrm{F}_{5/2}):\mathrm{Tb^{3+}}(^7\mathrm{F}_6) + \text{photon}$$
$$\Rightarrow \mathrm{Yb^{3+}}(^2\mathrm{F}_{7/2}):\mathrm{Tb^{3+}}(^5\mathrm{D}_4).$$

The fingerprints for this type of process are:

(1) immediate decay upon short-pulse excitation since the termination of the light also terminates the UC;
(2) transitions observed in the UC excitation spectra which do not match GSA transitions, i.e. ESA transitions.

The GSA/ESA mechanism has been well studied in many single-ion UC systems [6]. However, until recently no reports have conclusively shown an UC system where the GSA transition occurs on one ion followed by an ESA transition to a different ion [28, 29]. Valiente *et al* report on Yb–Mn pairs where the UC luminescence is attributed to GSA/ESA transitions within a single chromophore, namely an Yb–Mn dimer. This assignment was made on the basis of pulsed measurements which showed only decay, i.e. no rise, immediately following the excitation pulse into an $\mathrm{Yb^{3+}}\ ^2\mathrm{F}_{5/2}$ level. Excited-state excitation spectroscopy further verified this assignment. Our study will focus on similar experiments to establish the UC mechanism in $\mathrm{SrCl_2}$:Yb, Tb

*4.2.2. CW spectroscopy.* Excitation into the $\mathrm{Tb^{3+}}\ ^7\mathrm{F}_6 \rightarrow\ ^5\mathrm{D}_4$ or the $\mathrm{Yb^{3+}}\ ^2\mathrm{F}_{7/2} \rightarrow\ ^2\mathrm{F}_{5/2}$ absorption regions, figures 1 and 2, leads to visible-by-eye green $\mathrm{Tb^{3+}}$ luminescence with the same spectral features for $T = 100$ K and greater; see figure 5. The UC luminescence can therefore be readily assigned to $\mathrm{Tb^{3+}}\ ^5\mathrm{D}_4 \rightarrow\ ^7\mathrm{F}_J$ transitions. For temperatures below $T = 100$ K the UC emission changes colour from green to blue with strongly decreasing intensity. The UC luminescence spectrum changes accordingly with the $\mathrm{Tb^{3+}}$ luminescence decreasing in intensity by orders of magnitude (see figure 8), and a remaining very weak UC luminescence band located around 20 000 $\mathrm{cm^{-1}}$ (see figure 5). The broad emission around 20 000 $\mathrm{cm^{-1}}$ is readily assigned to the well-known Yb–Yb pair emission [30]. Additional features are observed at 18 000 and 15 000 $\mathrm{cm^{-1}}$ which we assign to $^4\mathrm{S}_{3/2} \rightarrow\ ^4\mathrm{I}_{15/2}$ and $^4\mathrm{F}_{9/2} \rightarrow\ ^4\mathrm{I}_{15/2}$ transitions, respectively, of trace $\mathrm{Er^{3+}}$ impurities present in the compound. Despite the use of 6N purity starting materials, trace amounts of $\mathrm{Er^{3+}}$ ions are present and appear in the UC emission spectrum due to the high efficiency of $\mathrm{Yb^{3+}}$-sensitized $\mathrm{Er^{3+}}$ UC luminescence [1, 31]. Many papers in the past have mistakenly reported $\mathrm{Er^{3+}}$ luminescence as $\mathrm{Tb^{3+}}$-ion or some other RE-ion luminescence under UC conditions. The Yb–Yb pair luminescence is also observed in the $T = 100$ K plot in figure 5 but has the dominant $\mathrm{Tb^{3+}}$ luminescence superimposed—see figure 8—at higher temperatures.

One possible explanation for the UC mechanism is the absorption of Yb–Yb luminescence by the $^7F_6 \rightarrow {}^5D_4$ transition of $Tb^{3+}$. However, the Yb–Yb pair luminescence has an observed $\frac{\text{VIS}}{\text{NIR}}$ ratio of $10^{-6}$ in $SrCl_2$ and in many other hosts [31]. The $Tb^{3+}$ UC luminescence is found to have a $\frac{\text{VIS}}{\text{NIR}}$ ratio starting below $10^{-8}$ at 10 K and increasing to $1 \times 10^{-4}$ (figure 1) at 100 K and finally $5 \times 10^{-4}$ at 300 K. Since these high-temperature values are significantly larger than for the Yb–Yb pair luminescence, this process can be eliminated. The following discussion of the cooperative UC mechanism in $SrCl_2$:Tb, Yb will focus on temperatures at and above 100 K.

The excitation spectrum of $Tb^{3+}$ UC luminescence at 100 K in figure 6 closely resembles the square of the $Yb^{3+}$ $^2F_{7/2} \rightarrow {}^2F_{5/2}$ transition ($GSA^2$). This is what is expected from an ETU mechanism—section 4.2.1—where the absorption which leads to UC only occurs to the intermediate meta-stable level. Also, since two excitations to the intermediate level are needed for bringing one $Tb^{3+}$ ion to the excited state, we find a power-dependent slope of 2 (figure 6(d)). More importantly, there are no extra transitions observed in the excitation spectrum which can be ascribed to an ESA step. If a GSA/ESA mechanism were the active UC process, there would be more than just the ground-state absorption transitions in the excitation spectrum.

*4.2.3. Dynamics.* To investigate this system further, we performed pulsed measurements. Time-dependent measurements also allow the distinction between a GSA/ESA mechanism, i.e. immediate decay, and a GSA/ETU process, i.e. rise from zero followed by decay; see section 4.2.1 [6]. The dynamic behaviour of cooperative sensitization corresponds to that of the ETU mechanism for more simple systems and can be treated in a similar manner. In particular, the cooperative sensitization relies on energy transfer from the two sensitizer ions to the activator and this process is relatively slow. Also, this process does not require the presence of light and therefore will continue after the pulse is terminated. For the Yb:Tb system the rise is expected to be related to half the $Yb^{3+}$ lifetime and the decay should be related to the $Tb^{3+}$ lifetime.

The UC luminescence temporal response for our system at 100 K after a short, 8 ns, pulse is given in figure 7. The luminescence intensity starts at zero, and this is followed by a rise and a decay. The rise is indicative of an energy transfer process and thus eliminates the possibility of a mechanism which involves an ESA step. The rise, shown in detail in figure 7(b), has a time constant of $\sim$150 $\mu$s and is thus shorter than the decay time, $\tau = 0.5$ ms, of the $Yb^{3+}$ ion; see table 1. Figure 7(c) displays the single-exponential behaviour of the UC luminescence decay which has a time constant of 2.1 ms which is slightly shorter than the lifetime, $\tau = 2.6$ ms, of the $Tb^{3+}$ under direct excitation; see table 1. The rise and decay will be discussed in more detail in section 4.2.4. This experiment, coupled with the excitation spectroscopy, allows the conclusive assignment of Yb:Tb UC luminescence at $T = 100$ K in $SrCl_2$:Yb, Tb to the cooperative sensitization mechanism.

*4.2.4. Model.* The transient data can be simulated by considering the cooperative sensitization mechanism shown schematically in figure 9. Using this diagram we can write down the four coupled differential rate equations describing the populations of each level, $N_i$:

$$\frac{dN_0}{dt} = -GN_0 + k_1N_1 + 2w_{CS}(N_1)^2N_2, \tag{1a}$$

$$\frac{dN_1}{dt} = GN_0 - k_1N_1 - 2w_{CS}(N_1)^2N_2, \tag{1b}$$

$$\frac{dN_2}{dt} = k_3N_3 - w_{CS}(N_1)^2N_2, \tag{1c}$$

$$\frac{dN_3}{dt} = -k_3N_3 + w_{CS}(N_1)^2N_2. \tag{1d}$$

**Table 2.** Decay rate constants of $Yb^{3+}$ and $Tb^{3+}$ at 100 K determined by square excitation (figure 4). The UC power-dependent rate constant was determined by fitting equations (1*a*)–(1*d*) to the experimental data in figure 7.

| Transition | | Decay rate constant ($s^{-1}$) |
|---|---|---|
| $^2F_{5/2} \rightarrow {}^2F_{7/2}$ | $k_1$ | 2020 (±50) |
| $^5D_4 \rightarrow {}^7F_6$ | $k_3$ | 400 (±5) |
| $^5D_4 \rightarrow {}^7F_6$[a] | $k_3^*$ | 470 (±5) |
| UC power-dependent rate constant[b] | $w_{CS}N_1N_2$ | 2000 (±500) |

[a] Decay rate determined under UC excitation conditions.
[b] Peak power $1 \times 10^7$ W mm$^{-2}$.

$k_1$ represents the $Yb^{3+}$ $^2F_{5/2}$ decay rate constant, $k_3$ the $Tb^{3+}$ $^5D_4$ decay rate constant, $G$ the power-dependent ground-state absorption rate constant, and $w_{CS}$ is the cooperative sensitization rate parameter. All the parameters in the figure and equations (1*a*)–(1*d*) are listed in table 2 and were determined from independent measurements—section 4.1—except for the energy transfer rate constant $w_{CS}N_1N_2$.

We use equations (1*a*)–(1*d*) to simulate the transient response of the UC luminescence after short-pulsed excitation into an $Yb^{3+}$ level. This simulation is plotted on top of the experimental data as a solid curve in figure 7. In this figure, and the insets, the simulation matches the experimental data with good agreement. In general the rise of the transient corresponds to the level possessing the shortest lifetime while the decay is related to the level with the longest lifetime. From table 1 we know that the $Yb^{3+}$ $^2F_{5/2}$ lifetime is shorter than the $Tb^{3+}$ $^5D_4$ lifetime and thus we expect the rise to be determined at least in part by the $Yb^{3+}$ $^2F_{5/2}$ lifetime. The decay is single exponential—figure 7(c)—and is of the order of the $Tb^{3+}$ $^5D_4$ lifetime. However, upon modelling the data, if one takes the value for $k_3$ determined in the direct excitation measurements, one finds that the simulation has values that are too high at the later times. For this reason we use the $k_3^*$-value determined from the square-wave UC decay transients—table 2—which has a 20% larger value than with direct excitation, i.e. a shorter lifetime. This difference is due to the selective nature of the UC measurement. UC excitation preferentially excites those $Tb^{3+}$ ions which are located near two $Yb^{3+}$ ions, whereas the direct excitation into the $Tb^{3+}$ $^5D_4$ level excites all $Tb^{3+}$ ions. The difference in lifetimes is due to the different local environments of the two sets of $Tb^{3+}$ ions. Under UC excitation we observe only the highly UC-active ions which are a small subset of the bulk of the impurity ions. This effect is often seen in doped systems where the UC-active subset of ions differs from the bulk ions [32]. Previous authors have also attributed this difference to an extra decay channel for the $Tb^{3+}$ ions near two $Yb^{3+}$ ions, namely cross-relaxation from one $Tb^{3+}$ to two $Yb^{3+}$ ions [21, 22, 25, 33].

From the rate equations it can be seen that the rise derives from the $Yb^{3+}$ lifetime and the power-dependent energy transfer UC rate constant $w_{CS}N_1N_2$. We report on the power-dependent rate constant instead of the power-independent parameter $w_{CS}$, because of the difficulties of measuring the initial number of excited $Yb^{3+}$ ions, $N_1$. We use the values from table 2 for the decay rate constants and vary the value of $w_{CS}N_1N_2$ to allow for the best simulation of the data. From this procedure we obtain a value of 2000 $s^{-1}$ for $w_{CS}N_1N_2$, with excitation at 10 192 cm$^{-1}$ and $1 \times 10^7$ W mm$^{-2}$. This will be discussed in more detail in the next section.

### *4.3. Upconversion efficiency and temperature dependence*

*4.3.1. Efficiency.* To discuss the quantum efficiency, $\eta = \frac{\mathrm{VIS}_{out}}{\mathrm{NIR}_{abs}}$, of this process we consider the ratio of VIS photons out to NIR photons out. As $Yb^{3+}$ has a quantum efficiency of 1,

we use the $Yb^{3+}$ luminescence to estimate the number of NIR photons absorbed. Thus, the quantum efficiency is approximated by the photon ratio $\frac{\mathrm{VIS}_{out}}{\mathrm{NIR}_{out}}$. For 100 K and CW excitation at 10 626 $cm^{-1}$ with 56 W $mm^{-2}$, we find a photon ratio of $1 \times 10^{-4}$. This photon ratio increases to $5 \times 10^{-4}$ at RT.

From this $\frac{\mathrm{VIS}}{\mathrm{NIR}}$ ratio at 100 K and equation (1*d*), one can estimate the $w_{CS}N_1N_2$ rate constant for a CW experiment:

$$\frac{w_{CS}N_1N_2}{k_1} = \frac{k_3N_3}{k_1N_1} = \frac{\mathrm{VIS}}{\mathrm{NIR}}. \tag{2}$$

Using these values we derive a value of $w_{CS}N_1N_2$ of 0.2 $s^{-1}$. This value determined for CW excitation is four orders of magnitude smaller than that found under pulsed excitation; see section 4.2.4. To account for this discrepancy in the estimated value of $w_{CS}N_1N_2$, we consider the differences between the two experiments used to estimate this value. In the pulsed experiment the peak power density is ∼5 orders of magnitude greater than in the CW measurement. Since the UC rate constant contains the number of ions excited during the NIR pulse, $N_1$, or written explicitly $N_1 = GN_0$, it is a power-dependent parameter. Thus, the UC rate constant, $w_{CS}N_1N_2$, increases with increasing power and is thus expected to be $\sim 1 \times 10^5$ times greater for the pulsed measurements. This value can be reduced from saturation effects. From our measurements we derive values differing by four orders of magnitude, in very good agreement with the theoretical expectations.

*4.3.2. Temperature dependence.* So far we have not discussed the energies of the levels involved in the CS process and what is required for UC to proceed. It is clear from the energies of the lowest excited states of both site A, 10 138 $cm^{-1}$, and B, 10 190 $cm^{-1}$, of $Yb^{3+}$ (figure 2(a)) that cooperative sensitization from two of these cannot populate the $Tb^{3+}$ $^5D_4$ level, 20 468 $cm^{-1}$ (figure 2(b)), at 10 K. There is a gap in energy of 192 and 88 $cm^{-1}$, for A and B respectively. And this is the main reason for the observed dramatic temperature dependence of the UC luminescence intensity.

The $Tb^{3+}$ $^5D_4$ emission intensity shows a very strong dependence on temperature especially in the region between 10 and 100 K, where it increases by more than two orders of magnitude with increasing temperature; figure 8(a). This strong temperature dependence has been quantified by analysing the integrated number of emitted photons as a function of inverse temperature; figure 8(b). The line drawn through the data is a linear regression using the Arrhenius equation (3):

$$\ln\left(\frac{I}{I_0}\right) = \frac{-\Delta E}{k_B T} \tag{3}$$

where $I$ represents the integrated emitted photons of $Tb^{3+}$, $\Delta E$ is the activation energy, $k_B$ is Boltzmann's constant, and $T$ is the temperature. The data are all normalized to the highest value of $I_0 = I(300\ \mathrm{K})$, and are corrected by the square of the absorption cross-section at $\tilde{\nu}_{exc} = 10\,626\ cm^{-1}$, at each temperature, as described in section 3. Analysis of these data yields a slope of $\Delta E = 150 \pm 12\ cm^{-1}$ for the activation energy of the UC luminescence intensity. This value is close to the energy mismatch between the lowest level of $Tb^{3+}$ $^5D_4$ at 20 468 $cm^{-1}$ and twice the lowest $Yb^{3+}$ $^2F_{5/2}$ level for both site A and site B. From this analysis it is clear that the cooperative sensitization process is facilitated only at higher temperatures where host phonons can contribute to the energy of the UC-active ions. At higher temperatures, vibronic $^2F_{5/2}$ levels of the $Yb^{3+}$ ions are thermally populated, from which the energy transfer can occur. Thus, from the temperature-dependent data, the excitation spectroscopy, and the dynamic measurements, the full assignment of phonon-assisted cooperative sensitization can be made for the mechanism of UC in this crystal.

## 5. Conclusions

The UC properties of $Yb^{3+}$-sensitized $Tb^{3+}$ luminescence has been investigated for many years. Despite this, many papers have been published concerning the UC mechanism of the Yb:Tb system with little agreement. We present results in this report where, for the first time, both standard techniques for determining UC mechanisms, namely excitation spectroscopy and time-resolved spectroscopy, have been coupled with temperature-dependent measurements to conclusively show a phonon-assisted cooperative sensitization mechanism governing the UC of Yb:Tb between 100 and 300 K. Many of the systems which are studied concerning Yb:Tb UC are similar to the $SrCl_2$ host. In this sense our result on $SrCl_2$ is a more general result applying to many crystals. The high efficiency of some Yb:Tb UC systems is also a sign that they are dominated by a cooperative sensitization process as opposed to a GSA/ESA process which is expected to be weaker, and is found to be of the order of the Yb–Yb pair luminescence in $Yb^{3+}$-doped $Cs_3Tb_2Br_9$ [5,34]. For the system of $SrCl_2$:Yb, Tb the cooperative sensitization is quenched at low temperatures due to the lack of spectral overlap between twice the $Yb^{3+}$ emission and the $^5D_4$ absorption at low temperatures. We have investigated the temperature dependence of the UC luminescence and determined the thermal activation energy of the cooperative sensitization. At temperatures where the cooperative sensitization is active, we have investigated the temporal behaviour by modelling the transient measurements with one adjustable parameter. The room temperature $\frac{\text{VIS}}{\text{NIR}}$ ratio of this system was found to be of the order of $10^{-4}$, but could be enhanced by an appropriate choice of dopant concentrations. However, enhancements by orders of magnitude are needed for an UC system which will yield efficient laser action. This paper, while specific to $SrCl_2$, suggests that the cooperative sensitization mechanism is the process most likely to be operative in efficient Yb:Tb systems.

## Acknowledgments

The authors thank Oliver Wenger for many interesting discussions and Karl Krämer for assistance in growing the crystals. This work was supported by the Swiss National Science Foundation.

## References

[1] Lenth W and Macfarlane R M 1992 *Opt. Photon. News* **3** 8
[2] Noginov M A, Venkateswarlu P and Mahdi M 1996 *J. Opt. Soc. Am.* B **13** 735
[3] Qiu J, Shojiza M, Kawamoto Y and Kadono K 2000 *J. Lumin.* **86** 23–31
[4] Livanova L D, Saitkulov I G and Stolov A L 1969 *Sov. Phys.–Solid State* **11** 750
[5] Salley G M, Valiente R and Güdel H U 2001 *J. Lumin.* **94–5** 305
[6] Gamelin D R and Güdel H U 2001 *Top. Curr. Chem.* **214** 1
[7] Tallant D R, Moore D S and Wright J C 1977 *J. Chem. Phys.* **67** 2897
[8] Kushida T 1973 *J. Phys. Soc. Japan* **34** 1334
[9] Reed J B, Hopkins B S and Audrieth L F 1936 *Inorg. Synth.* **1** 28
[10] Meyer G 1989 *Inorg. Synth.* **25** 146
[11] Carnall W T, Fields P R and Rajnak K 1968 *J. Chem. Phys.* **49** 4412
[12] Piper T S, Brown J P and McClure D S 1967 *J. Chem. Phys.* **46** 1353
[13] Wietfeldt J R and Wright J C 1987 *J. Chem. Phys.* **86** 400
[14] Jones G D and Murdoch K M 1994 *J. Lumin.* **60–1** 131
[15] Tanner P A, Ravi Kanth Kumar V V, Jayasankar C K and Reid M F 1994 *J. Alloys Compounds* **215** 349
[16] Richardson F S, Reid M F, Dallara J J and Smith R D 1985 *J. Chem. Phys.* **83** 3813
[17] Schwartz R W, Brittain H G, Riehl J P, Zeakel W and Richardson F S 1977 *Mol. Phys.* **34** 361
[18] Voron'ko Yu K, Osiko V V and Shcherbakov I A 1969 *Sov. Phys.–JETP* **29** 86

[19] Dieke G H 1968 *Spectra and Energy Levels of Rare Earth Ions in Crystals* (New York: Interscience)
[20] Ovsyankin V V and Feofilov P P 1966 *JETP Lett.* **3** 317
[21] Ostermayer F W and van Uitert L G 1970 *Phys. Rev.* B **1** 4208
[22] Antipenko B M, Dmitryuk A V, Karapetyan G O, Zubkova U S, Kosyakov V I, Mak A A and Mishailova N V 1973 *Opt. Spectrosc.* **35** 315
[23] Brown R S, Brocklesby W S, Barnes W L and Townsend J E 1995 *J. Lumin.* **63** 1
[24] Adam J L, Duhamel-Henry N and Allain J Y 1997 *J. Non-Cryst. Solids* **213–14** 245
[25] Strek W, Deren P and Bednarkiewicz A 2000 *J. Lumin.* **87–9** 999
[26] Martín I R, Yáñes A C, Mendez-Ramos J, Torres M E and Rodriguez V D 2001 *J. Appl. Phys.* **89** 2520
[27] Bilak V I, Zverev G M, Karapetyan G O and Onischenko A M 1971 *JETP Lett.* **14** 199
[28] Valiente R, Wenger O S and Güdel H U 2001 *Phys. Rev.* B **63** 165102-1
[29] Valiente R, Wenger O S and Güdel H U 2000 *Chem. Phys. Lett.* **320** 639
[30] Nakazawa and Shiyonoya 1970 *Phys. Rev. Lett.* **25** 1710
[31] Goldner Ph, Pellé F, Meichenin D and Auzel F 1997 *J. Lumin.* **71** 137
[32] Gamelin D R and Güdel H U 1999 *Inorg. Chem.* **38** 5154
[33] Strek W, Bednarkiewicz A and Deren P J 2001 *J. Lumin.* **92** 229
[34] Salley G M and Güdel H U 2002 *Phys. Rev.* B at press